Available online at www.sciencedirect.com
ScienceDirect
Journal of Nuclear Materials 366 (2007) 161–177
journal of nuclear materials
www.elsevier.com/locate/jnucmat

Comparison of interatomic potentials for UO_2. Part I: Static calculations

K. Govers [a,b,*], S. Lemehov [b], M. Hou [c], M. Verwerft [b]

[a] Service de Métrologie Nucléaire (CP 165/84), Université Libre de Bruxelles, 50 av. F.D. Roosevelt, B-1050 Bruxelles, Belgium
[b] Reactor Material Research Department, SCK·CEN, Boeretang 200, B-2400 Mol, Belgium
[c] Physique des Solides Irradiés et des Nanostructures (CP 234), Université Libre de Bruxelles, Bd du Triomphe, B-1050 Bruxelles, Belgium

Received 6 June 2006; accepted 10 December 2006

Abstract

An improved knowledge of nuclear fuel can be gained from a better description of atomic-scale processes such as point defects behaviour under irradiation. In this perspective the different techniques involving interatomic potentials can play a major role as they permit to simulate such mechanisms at the atomic scale. In this article we will assess the range of applicability of the available interatomic potentials for UO_2 by static calculations. Lattice properties have been envisaged, together with defect properties: the formation and activation energies of vacancies and interstitials, the binding energy of small clusters of these defects and the volume change associated with them.

PACS: 31.15.Qg; 34.20.Cf; 61.72.−y; 61.72.Ji; 66.30.Hs; 71.15.Pd; 83.10.Rp

1. Introduction

Fuel rod behaviour under irradiation is affected by many phenomena, and it is sometimes very difficult to isolate each process by experimental means. From a technical point of view, this is not limiting for UO_2, since more than 40 years of experiments have permitted to create useful correlation curves. The extension of this knowledge to new types of fuels, for which less experiments have been conducted, requires an improved multi-scale modelling of these processes based on the understanding of elementary processes at the atomic scale.

A significant step forward in their understanding may be expected thanks to two techniques based on interatomic potentials describing the interactions of atoms. Energy minimisation allows to assess the stability of specific configurations after lattice relaxation. Molecular dynamics (MD) allows to determine the time-evolution of a set of interacting atoms. It is limited in system size (up to a few million atoms) and time (up to a few nanoseconds). Energy minimisation can be achieved in a few iterations with hessian-based algorithms for which the memory needs increase very rapidly with system size. A system containing of the order of 1000 atoms

* Corresponding author. Address: Service de Métrologie Nucléaire (CP 165/84), Université Libre de Bruxelles, 50 av. F.D. Roosevelt, B-1050 Bruxelles, Belgium.
E-mail address: kgovers@sckcen.be (K. Govers).

0022-3115/$ - see front matter © 2007 Elsevier B.V. All rights reserved.
doi:10.1016/j.jnucmat.2006.12.070

is generally a good compromise for isolated defects. Much larger systems can be considered if gradient-based techniques are used, but with a larger number of iterations.

A number of interatomic potentials describing the interactions in UO_2 have been developed over the past decades. Several authors have fitted an interatomic potentials on different experimental data. The aim of this article is to make a broad comparison of these potentials, helping this way to appreciate their range of applicability. Lattice properties (lattice parameter, elastic constants, dielectric constants, phonon frequencies at Γ point) and defect properties (energy, stability, migration and swelling) estimated with these potentials will be compared to experiment and ab initio predictions. MD simulations of dynamical properties will be reported in a subsequent article.

Section 2 introduces the different descriptions of interatomic potentials (Section 2.1). It is followed by a review on pair potentials for UO_2 (Section 2.2). Section 2.3 provides an overview of the different calculation techniques used and how to compare them to experimental results. A discussion of the results is proposed in Section 3. Results are synthesized in Section 4.

2. Methodology

2.1. Pair potentials survey

Two main categories of interatomic potentials have been developed in the past. In the first one, polarization effects are taken into account by means of the shell–core model of Dick and Overhauser [1]. Ions are described as a massless charged shell bound to a massive core by a spring. Note that the interatomic potential acts between the shells, except for the Coulomb interaction that acts between both shells and cores. In the second model, the rigid ion model, ions are considered as massive point charges. MD simulations with this more simplified model are faster because the shell motion (which is more rapid due to the zero mass of shells) is absent.

The usual form of the pair potential in oxides consists into the addition of a Buckingham form to the Coulomb potential

$$V_{ij}(r) = \frac{q_i q_j e^2}{4\pi\varepsilon_0} + A_{ij}\exp\left(-\frac{r}{\rho_{ij}}\right) - \frac{C_{ij}}{r^6}, \tag{1}$$

where r is the distance between atoms i and j.

In order to avoid the unphysical attractive forces at very short distance, a 'Buckingham-4 ranges' has been proposed, defined by intervals

$$V_{ij}(r) = \frac{q_i q_j e^2}{4\pi\varepsilon_0} + \begin{cases} A_{ij}\exp\left(-\frac{r}{\rho_{ij}}\right) & \text{if } r \leqslant r_1, \\ \text{5th-degree polynom} & \text{if } r_1 < r \leqslant r_{\min}, \\ \text{3rd-degree polynom} & \text{if } r_{\min} < r \leqslant r_2, \\ -\frac{C_{ij}}{r^6} & \text{if } r > r_2. \end{cases} \tag{2}$$

The two splines are such that the potential and its two first derivatives are continuous and that $r_{\min}$ is the potential minimum.

Another form of potential for oxides has been developed in order to model covalent bounds between anions and cations. It consists of the addition of a Morse potential (describing the covalent bound) to the Buckingham potential acting between anions and cations. Anion–anion and cation–cation interactions remain of the Buckingham form. Charges of ions are generally a fraction of the formal charges with such a model. The potential is then expressed by

$$V_{ij}(r) = \frac{q_i q_j e^2}{4\pi\varepsilon_0} + f_0(b_i + b_j)\exp\left(\frac{a_i + a_j - r}{b_i + b_j}\right) - \frac{c_i c_j}{r^6} + D_{ij}\left\{\left[1 - \exp\left(\beta_{ij}(r - r^*_{ij})\right)\right]^2 - 1\right\}. \tag{3}$$

All short-range potentials were used in this work with a cut-off at 10.4 Å while the Coulomb interactions were treated with the classical Ewald summation technique.

2.2. Pair potentials development

This section will present, as much as possible in a chronological way, the interatomic potentials developed for UO_2, and their use in other work. We will refer to the potentials by the name of their first author and a digit if they created more than one, e.g. Catlow1 and Catlow2, except for the potentials created by Lewis and Catlow (see further) that are widely known as 'Lewis_a, b or c'.

The first article where an interatomic potential was established for UO_2 was written in 1962 by Benson et al. [2]; it was based on a rigid ion description, and fitted to lattice parameter and compressibility data. This potential was used to calculate the cohesive energy of the crystal. A few years later a second article appeared, written by Dolling et al. [3]. Four sets of potentials were established, based

on a fitting to dispersion curves. One of these was based on a rigid ion description, the other ones on the shell–core model of Dick and Overhauser [1]. Unfortunately the authors of these two articles did not mention the values of the different parameters of the potentials.

The first available sets of parameters for the UO_2 systems, developed by Tharmalingam [4], were fitted on elastic properties, and used in order to calculate point defect energies. The calculations were done using the point polarizable ion model, which according to Catlow and Norgett [5], can show instabilities in the calculation of dipoles interaction. Note that for the second set (Tharmalingam2), the author added to the usual Buckingham form a $-D/r^8$ term.

In the 70s Catlow started a series of articles on UO_2 [5–7] where different interatomic potentials were developed. In Ref. [6] two potentials for UO_2, based on a shell–core description, were developed by fitting to elastic and dielectric constants and lattice parameter. They were designed to calculate formation energies of point defects. One of these two potentials, Catlow1, was also used by Sugisaki [8] in order to calculate the enthalpy of solution of MgO in UO_2, and both of them by Abramowski et al. [9] in order to study the grain growth of UO_2.

Based on this work a rigid ion potential has been developed by Walker and Catlow [10], adjusting the U–O potential parameters in order to predict correctly the static dielectric constant and lattice parameter. A rigid ion potential was needed in order to make molecular dynamics simulations (much less time consuming than shell–core potentials) of properties of UO_2 at high temperatures (transition to superionic phase). Walker's potential was more recently used by Motoyama et al. [11] for the calculation of the thermal conductivity of UO_2. A few years later, in 1985, Lewis and Catlow [12] developed their well-known libraries of potentials adapted for several metal oxides, among which UO_2. For each library the same O–O interaction is kept, allowing to simulate alloys of these oxides. Three sets can be found in their paper concerning uranium dioxide, the first one is a rigid ion potential, the two others being shell–core potentials.

The same year Jackson et al. [13] modified the Catlow1 potential [6], using a polynomial interpolation at intermediate separation (Eq. (2)), in order to correct the unphysical behaviour of the Buckingham-type potential at very low separations – the potential becomes attractive at very low distance because of the $1/r^6$ term. These authors also developed a second potential (referred as Jackson2) that takes dynamical effects into account (the thermal expansion). The aim of their study was to calculate defect formation energies, substitution energies (for U^{2+}, U^{3+}, U^{5+}, U^{6+}, Ce^{3+}, Ce^{4+}, Pu^{2+}, Pu^{3+}, Pu^{4+}, Pu^{5+}, and Pu^{6+}) and activation energies in UO_2, using the quasi-harmonic approximation for temperatures above 0 K. They also determined phonon dispersion curves. The second potential was used in other articles of Jackson: Jackson et al. [14] where defect formation energies were calculated; and Jackson and Catlow [15,16] where the solution energy of Xe was calculated.

Lindan and Gillan [17] used the Jackson2 potential to make the first shell–core MD simulations of UO_2 in 1994. They studied oxygen diffusion at high temperature and the apparition of the superionic phase. These results were in good agreement with previous rigid ion model simulations. Jackson2 potential was subsequently used by Nicoll et al. [18,19] to study respectively Xe and Mo solution in UO_2; and by Abramowski et al. [9] for the grain growth of UO_2.

A series of rigid ion potential is based on Jackson2, again in order to make more rapid molecular dynamics simulations. Sindzingre and Gillan [20] modified the O–U potential such that the lattice parameter and oxygen Frenkel pair energy remains the same as for Jackson2, keeping the original O–O interaction. They simulated by MD oxygen diffusion at high temperatures, lattice thermal expansion, specific heat and the melting point. This potential was then used by Gillan [21] to study the diffusion coefficient at different temperatures; and by Lindan and Gillan [22] to study thermal conductivity, also using MD. Sindzingre potential showed an instability (softening of one Raman mode) and was for that reason slightly modified by Karakasidis and Lindan [23]. The fitting kept the oxygen Frenkel pair formation energy value calculated with the Jackson2 potential. Karakasidis and Lindan used MD in order to simulate the superionic transition.

A new modification of this potential was made by Morelon et al. [24], in order to reproduce more accurately defect properties. The fitting was for this reason based on defect energies and lattice parameter. For this potential, ions have no longer their formal charges (i.e. not +4 and −2 for respectively U and O ions). They calculated various defect formation and activation energies. This potential was developed in order to simulate displacement cascades in UO_2 (see [25]).

In parallel to this, Grimes and Catlow produced a consistent set of interatomic potential (shell–core model) for UO_2 and several impurities. The fitting of the potentials was based on electron-gas calculations. In a set of articles [26,27] the solution energies of Xe, I, Ba, Kr, Rb, Br were studied. In a subsequent paper [28], migration and solution energies of Br, Kr, Rb, Sr, Y, Te, I, Xe, Cs, Ba, La, Ce are calculated. He behaviour was studied by Grimes et al. in [29]. The Grimes potential has also been used by Ball and Grimes [30] in order to study solution and activation energies of Xe in UO_2; by Grimes et al. [31] for I and Cs; by Grimes in [32] for Br, Kr, Rb, Sr, Y, Zr, Te, I, Xe, Cs, Ba, La, Ce; by Abramowski et al. [9] for the study of grain growth; and by Busker et al. [33,34] for respectively the diffusion of I and Cs in UO_2 and the solution and diffusion of Ru in UO_2.

In their article Abramowski et al. [9] also give the parameterisation for another set of potentials, created by Busker. It is referred as a private communication. We decided to use this potential in this study, even if no original article written by Busker about this potential could be found in the literature.

Recently a Japanese group developed a series of rigid ion potentials for nuclear fuels, a.o. UO_2 [35], $(U,Pu)O_2$ [36], minor actinides oxides [37,38], and also for several nitrides [39–41]. The fitting of these potentials was based on lattice parameter and bulk modulus evolutions with temperature; using non-formal charges. Note that this Japanese group added a Morse-type potential to the Buckingham-type potential. The same O–O potential is used for every system, and this formalism allows to consider mixing of compounds (in order to simulate e.g. MOX fuel). Yamada's fitting has been subsequently improved by Basak et al. [42] using isothermal compressibility data in order to reproduce more accurately the lattice expansion.

In 2005 Arima et al. [43] published two sets of rigid ion potentials, having the usual Buckingham form, formal charges for the first set, the other set having non-formal charges. The formalism used was the same as for the potential developed by the Japanese group of Yamada, each ion having its own parameters (see Eq. (3)). It is thus possible to use the parameters of UO_2 and of PuO_2 to obtain the U–Pu interaction and thus to simulate $(U,Pu)O_2$.

Meis and Gale [44] studied lattice diffusion of U and Pu in zirconium orthosilicate ($ZrSiO_4$). They developed a set of interatomic potentials (shell–core model) for zircon, UO_2 and PuO_2 and then transferred the obtained U–O and Pu–O potentials to zircon. Their fitting was based on lattice parameter, elastic tensor elements, static and dielectric constants as well as piezoelectric constants, constraining oxygen's shell and core charges to be identical in all three ionic structures (in order to transfer the potentials from UO_2 and PuO_2 to $ZrSiO_4$). Finally the last potential (shell–core model) used in our study was developed by Meis and Chartier [45]. The fitting was based on crystallographic, elastic and dielectric properties of UO_2. Then the set of potentials was used to calculate thermodynamic properties, Frenkel pair formation energies and migration energies. If these properties were not well reproduced, a new parameterisation was established changing the initial values of the fitted parameters.

The parameterisation of the potentials can be found in Tables 1–3 for respectively the shell–core model potentials, the rigid ion potentials with Buckingham form and the rigid ion potentials with Buckingham + Morse form. All parameters have been converted using eV and Å units for clarity.

2.3. Calculation techniques and comparison to experimental data

2.3.1. Energy minimisation strategies

The calculations in this article involve two energy minimisation strategies. The first explores global energy maps using periodic boundary conditions (PBC). The second, due to Mott and Littleton privileges a local approach [46]. Both methods which are implemented in the GULP code [47], were used in this study. These energy minimisation techniques search stationary points at which gradients are zero. If the number of imaginary eigen-values of the hessian is zero, then a local minimum has been found. Stationary points with imaginary eigen-values correspond to energy saddle point. They have also been computed, in order to determine migration energies of atoms. In the periodic boundary conditions approach, energy minima are searched using the BFGS (Broyden, Fletcher, Goldfarb and Shanno) algorithm implemented in GULP [47].

For systems containing one or more defects, because of the periodic boundary conditions, atoms interact not only with the original defect(s) but also with its (their) images generated by these boundary conditions. In order to make this undesirable effect negligeable, the size of the simulation box must be large enough. The BFGS algorithm may then

Table 1
Parameters of the shell–core potentials of the form of Eq. (1) or (2)

Parameters	Units	Potentials									
		Busker [9]	Catlow1 [6]	Catlow2 [6]	Grimes [28]	Jackson1[a] [14]	Jackson2 [14]	Lewis_b [12]	Lewis_c [12]	Meis1 [44]	Meis2 [45]
Charges											
O shell	e	−2.08	−4.4	−3.06	−4.4	−4.4	−4.4	−2.7	−3	−2.86	3.18627
O core	e	0.08	2.4	1.14	2.4	2.4	2.4	0.7	1	0.86	1.18627
O spring	eV/Å^2	6.3	292.98	80.21	296.8	292.98	296.2	51.6	49.5	52.308	70.824
U shell	e	−0.1	6.54	7.94	6.54	6.54	6.54	6.44	5.35	/	−2.84
U core	e	4.1	−2.54	−4.1	−2.54	−2.54	−2.54	−2.44	−1.35	4	6.84
U spring	eV/Å^2	160	103.38	210.02	98.24	103.38	94.24	129	109.7	/	171.556
Parameters: O–O interactions											
A	eV	9547.96	22764.3	22764.3	108	20378	11272.6	22764.3	22764.3	22764.3	20908.03
ρ	Å	0.2192	0.149	0.149	0.38	0.12537	0.1363	0.149	0.149	0.149	0.1296
C	eV Å^6	32	112.2	20.37	56.06	114	134	112.2	112.2	31.984	229.04
Spline											
r_1	Å					1.159	1.2				1.17
r_{min}	Å					1.65	2.1				1.62
r_2	Å					2.7299	2.6				2.84
Parameters: O–U interactions											
A	eV	1761.775	1217.8	1297.44	2494.2	1217.8	1518.92	1055.5	1014.3	841	844.41
ρ	Å	0.35642	0.3871	0.3747	0.34123	0.3871	0.38208	0.3949	0.3976	0.4169	0.425243
C	eV Å^6				40.16		65.41				
Parameters: U–U interactions											
A	eV				18 600						
ρ	Å				0.27468						
C	eV Å^6				32.64						

The short-range potentials act between shells only.
[a] In the original paper the splines of Jackson1 and Jackson2 potentials are of the 7th order between r_{min} and r_2.

Table 2
Parameters of the rigid ion potentials of the form of Eq. (1) or (2)

Parameters	Units	Potentials							
		Arima1 [43]	Karakasidis [23]	Lewis_a [12]	Morelon [24]	Sindzingre [20]	Tharmalingam1 [4]	Tharmalingam2[a] [4]	Walker [10]
O charge	e	−2	−2	−2	−1.61363	−2	−2	−2	−2
U charge	e	4	4	4	3.227252	4	4	4	4
Parameters: O–O interactions									
A	eV	22517.53[b]	11272.6	22764.3	11272.6	11272.6	−93.3	36.1	50259.34
ρ	Å	0.149	0.1363	0.149	0.1363	0.1363	0.398	0.382	0.15285
C	eV Å^6	27.59	134	112.2	134	134		27	72.65339
Spline									
r_1	Å		1.2		1.2	1.2			
$r_{\min}$	Å		2.1		2.1	2.1			
r_2	Å		2.6		2.6	2.6			
Parameters: O–U interactions									
A	eV	1133.05	895.5898	1055	566.498	869.98	959.6	1371	873.3274
ρ	Å	0.386	0.42512	0.3949	0.42056	0.427	0.398	0.382	0.40369
C	eV Å^6		−65.4			−65.4		53	

[a] For Tharmalingam2 potential; supplementary terms are added to the Buckingham form: $a - D/r^8$ term. The value of D (in eV Å^8) is 19 for O–O interaction; 159 for O–U; and 1721 for U–U. The parameter C has also a non-zero value for the U–U interaction: 231 eV Å^6.

[b] We think that this parameter was originally taken from Catlow's work (22764.3 eV) but slightly modified by conversion factors to kJ/mol and inversely.

Table 3
Parameters of the rigid ion potentials of the form of Eq. (3)

Parameters	Units	Potentials		
		Arima2 [43]	Basak [42]	Yamada [35]
f_0	eV/Å	0.043405	0.04222	0.043405
Parameters for O				
Charge	e	−1.35	−1.2	−1.2
a	Å	1.847	1.91	1.926
b	Å	0.166	0.163511	0.16
c	$eV^{1/2}/Å^3$	4.1668	1.98762	2.03657
Parameters for U				
Charge	e	2.7	2.4	2.4
a	Å	1.318	1.63	1.659
b	Å	0.036	0.16351	0.16
c	$eV^{1/2}/Å^3$	0	0	0
Parameters for O–U interaction				
D_{ij}	eV		0.57745	0.78129
r^*	Å		2.369	2.369
β_{ij}	1/Å		1.65	1.25

become too time-consuming and a conjugate gradient algorithm is preferable. The latter approach is used in this article in order to estimate the swelling due to defects, because energy minimisation with PBC allows to work at constant pressure. Convergence of energy was reached for a system consisting of $4 \times 4 \times 4$ conventional unit cells (768 atoms).

According to the Mott–Littleton approach [46], the environment around the defect is divided in three regions by two concentric spheres. Inside the smallest one, ions are strongly affected by the presence of the defect and interactions are calculated explicitly with a full relaxation of the lattice. In the intermediate region, atoms are weakly perturbed, leading to an harmonic relaxation. The outside region is treated as a dielectric medium. Both energy minima – corresponding to stable defect configurations – and energy saddle point – corresponding to the migration of atoms – can be considered with this approach. Saddle points are calculated using the RFO (Rational Function Optimisation) [48] procedure. Since the migration energy is the difference between the energy at a saddle point and at the minimum, the Mott–Littleton approach is very attractive.

Both methods predicts the same formation energy if the system size is sufficient, but the Mott–Littleton method seems to converge faster (i.e. with smaller systems) and offers the best compromise on computer time. The radii of the spheres used in this article were of 9 and 20 Å.

2.3.2. Elastic properties

Once the minimum energy configuration has been found, different crystallographic, elastic and dielectric properties of the crystal can be estimated at 0 K from the second derivatives of the potential. The experimental elastic properties, however, are obtained at room temperature and defect energies at even higher temperatures. The comparison is nevertheless valid insofar both defect energies and elastic data are not strongly varying with temperature in the range of interest. The 0 K lattice parameter, however, has to be estimated by extrapolation to 0 K. An illustration of the UO_2 lattice can be found in Fig. 1.

Experimental elastic data used for the comparison can be found in: [49–51] (lattice parameter – a_0, thermal expansion), [51–58] (elastic constants – C_{11}, C_{12}, C_{44}, bulk modulus – B, Young modulus – E, Poisson's ratio – v); dielectric data from: [6,59] (static dielectric constant – ε_0, high frequency dielectric constant – ε_∞); phonon frequencies at Γ point from: [3].

2.3.3. Defect formation energies

As previously mentioned, defect energies were estimated using the Mott–Littleton approach. Experimental values of defect formation energies can be found in: [50,52,53,60–64] (oxygen Frenkel pair – OFP), [61,65,66] (uranium Frenkel pair – UFP). The energies obtained in this work can also be compared to ab initio calculations (see e.g. [67–72]).

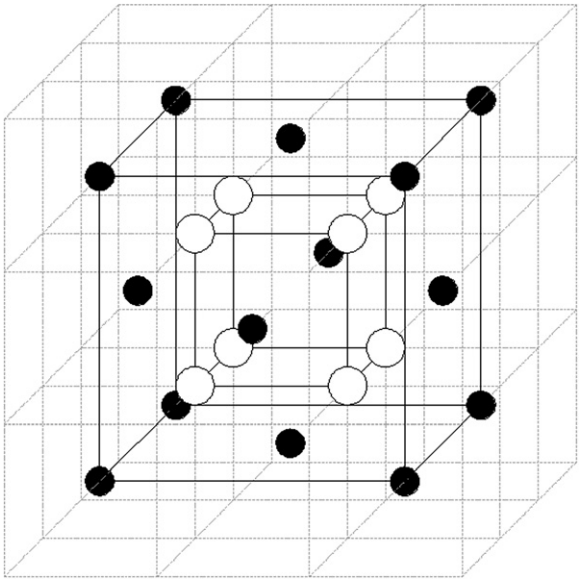

Fig. 1. UO_2 lattice. Dark spheres are U atoms. O atoms are situated at each gray cube edge, but are only shown as white spheres in the central zone for clarity reasons.

Care has to be taken for defects that does not conserve the stoichiometry of the system, such as vacancies or interstitials. In that case their formation energy (the energy appearing in the Boltzmann expression of their concentration as a function of the temperature) is not simply equal to the energy difference between the 'undefective' system and the 'defective' system (called Grand canonical energy parameter in [73], E_{gc}). Mayer and Fahnle [73] have demonstrated that in the case of an ordered alloy where the dominant defects are vacancies and antisites, the vacancy formation energy could be expressed as $E_f = E_{gc} + \mu_0$, where μ_0 is the chemical potential of the species. Similarly the relaxation volume of these defects has to be corrected. The case of uranium dioxide would be still more difficult to envisage, as interstitial defects are situated on a separate sublattice than U and O ones.

The comparison of semi-empirical estimation of E_{gc} to ab initio data is also not straightforward because the reference energies are different in the two methods when considering charged defects – oxygen vacancy (V_O), uranium vacancy (V_U), oxygen interstitial (O_I) or uranium interstitial (U_I) – e.g. the formation energy of an oxygen vacancy:

- with ab initio, the atom at 'infinity' can be chosen as atomic O or $\frac{1}{2}O_2$;
- with the semi-empirical potentials (used in MD) a charged ion is brought to infinity. One point to note is that O^{2-} is unbound in vacuum, which implies that the difference between the two referentials has to be estimated. An estimations of this value has been made [8,67], but its extension to non-formal charges e.g. $O^{1.2-}$ requires an hypothesis on the evolution of atomic energy with non-integer charges.

This problem does not occur with intrinsic defects (which are neutral): Frenkel pairs (FP) or Schottky defects (Sch in Table 4). The other possibility is to consider differences of energy in the same particular referential: binding energies of several defects (divacancies: $V_O + V_O$ or $V_O + V_U$, tetravacancies – denoted 4-vac. in Table 4: $2V_O + 2V_U$) or migration energies.

Properties of small clusters of defect have also been evaluated, for which no experimental data are available for comparison: close Frenkel pairs, di-interstitials of oxygen, divacancies, trivacancies and tetravacancies binding energies. In the case of oxygen Frenkel pairs, we observed that moving a regular oxygen atom to the closest interstitial site (center of an oxygen cube) resulted in a direct recombination of the two defect. Gupta et al. [72] obtained by ab initio calculation a value of 0.1 eV for this configuration. Therefore two other situations were considered:

- The vacancy and the interstitial are separated by a (lattice) U atom: the vacancy is in $-\frac{1}{4}, -\frac{1}{4}, -\frac{1}{4}$; the lattice U atom in 0, 0, 0 and the interstitial in $\frac{1}{2}, \frac{1}{2}, \frac{1}{2}$. This avoided recombination during lattice relaxation. This situation is referred as OFP 1.
- The same situation except that the vacancy is in $-\frac{1}{4}, -\frac{1}{4}, +\frac{1}{4}$. This situation is referred as OFP 2.

The oxygen Frenkel pair energy at infinite distance (OFP_∞) is just the sum of the energies of a vacancy and an interstitial. Three types of Schottky defects were also considered (an illustration is provided in Fig. 2), the uranium vacancy being in 0, 0, 0; the first oxygen vacancy in $+\frac{1}{4}, +\frac{1}{4}, +\frac{1}{4}$ and the second oxygen vacancy in $-\frac{1}{4}, -\frac{1}{4}, -\frac{1}{4}$ (Sch 1), in $-\frac{1}{4}, \frac{1}{4}, -\frac{1}{4}$ (Sch 2), in $-\frac{1}{4}, \frac{1}{4}, \frac{1}{4}$ (Sch 3). Divacancies and tetravacancies were considered as the smallest possible cluster of vacancies.

Table 4
Properties calculated with the different potentials for spheres radii in the Mott–Littleton method of 9 and 20 Å

	Units	Potentials																			
		Ar.1 [43]	Bas. [42]	Bus. [9]	Ca.1 [6]	Ca.2 [6]	Gri. [28]	Ja.1 [14]	Ja.2 [14]	Kar. [23]	Le.a [12]	Le.b [12]	Le.c [12]	Me.1 [44]	Me.2 [45]	Mor. [24]	Sin. [20]	Th.1 [4]	Wal. [10]	Yam. [35]	Exp. or ab initio [3,49–71,74–77]
$E_{coh.}$	eV	103.0	43.2	104.5	103.1	94.5	105.7	103.1	103.5	100.6	103.6	103.6	103.6	99.9	100.8	65.9	100.8	103.0	104.1	45.6	
a_0	Å	5.454	5.454	5.468	5.451	5.521	5.462	5.448	5.452	5.466	5.389	5.390	5.382	5.559	5.469	5.447	5.449	5.410	5.328	5.467	5.4552 (extrapol.)
C_{11}	GPa	479.8	408.1	532.1	420.1	434.4	524.2	421.2	398.4	369.3	427.0	426.8	426.9	432.3	389.2	217.1	370.7	472.8	471.0	419.5	389.3
C_{12}	GPa	101.9	61.2	122.3	125.7	100.4	147.3	126.5	132.4	87.8	121.5	121.4	119.3	77.9	118.6	79.0	86.3	96.4	102.6	59.4	118.7
C_{44}	GPa	95.5	59.5	118.8	66.2	57.3	89.2	66.8	73.8	70.3	119.4	88.5	49.9	24.2	59.6	78.4	65.6	84.3	89.4	54.7	59.7
B	GPa	227.9	176.9	258.9	223.8	211.8	272.9	224.9	221.0	181.6	223.3	223.2	221.8	196.0	208.8	125.0	181.1	221.9	225.4	179.4	204.0
E	GPa	444.3	392.2	486.4	362.2	396.7	459.6	363.3	332.4	335.6	373.2	373.0	374.8	408.6	333.8	174.9	338.1	440.1	434.3	404.7	385.0
ν		0.18	0.13	0.19	0.23	0.19	0.22	0.23	0.25	0.19	0.22	0.22	0.22	0.15	0.23	0.27	0.19	0.17	0.18	0.12	
ε		11.1	4.0	18.4	20.9	25.4	13.1	20.8	19.8	18.4	9.9	17.8	17.5	23.1	24.0	10.2	20.1	13.7	14.4	3.8	24.0
ε_∞				6.2	5.4	5.2	5.3	5.4	5.8			5.4	5.4	2.6	5.3						5.3
Phonons at Γ																					
T. mode	cm^{-1}	260.5	289.4	183.3	273.7	235.8	343.9	274.8	287.8	198.4	282.6	274.0	271.4	194.3	245.1	221.1	190.0	235.9	235.1	294.7	280.0
L. mode	cm^{-1}	493.6	577.1	282.2	444.9	447.1	533.2	446.9	434.6	381.6	443.4	400.7	396.6	411.3	413.2	287.7	377.4	473.5	457.5	616.2	450.0
Formation energies																					
O FP_∞	eV	6.9	6.0	6.4	5.1	5.1	6.9	5.2	4.9	4.9	6.8	5.4	5.3	4.0	4.6	3.9	4.7	6.2	6.0	6.0	3.6–3.9[a]
OFP1[b]	eV	5.6	5.2	5.5	3.7	3.7	5.8	3.7	3.9	3.8	5.5	4.2	4.0	Rec.	1.3	3.1	3.6	5.0	4.8	5.2	3.63[a]
OFP2[b]	eV	5.5	4.8	5.5	[d]	4.1	5.8	4.3	4.0	3.8	5.4	4.4	4.2	[d]	3.1	3.0	3.5	4.9	4.8	4.7	3.1–5.4
UFP_∞	eV	24.5	17.0	22.4	18.8	16.7	24.1	19.0	19.2	19.5	25.5	20.4	19.2	17.7	18.6	15.7	19.0	22.4	22.3	18.5	9.5–12.6[a]
UFP[b]	eV	6.4	12.4	[d]	14.5	13.0	18.7	14.8	14.7	15.1	[d]	15.9	14.5	13.4	15.8	11.9	[d]	17.2	16.4	13.9	8.5–9.6, 6.09[a]
$Sch._\infty$	eV	10.2	10.8	10.8	9.8	7.4	13.4	10.0	11.1	7.0	12.6	9.8	9.2	4.2	9.7	8.0	6.3	8.1	8.3	13.5	4.9–6[a]
Sch.1	eV	4.8	5.4	6.2	5.4	4.1	7.3	5.5	6.4	3.4	6.2	5.4	4.6	1.3	5.5	4.1	3.0	3.6	3.8	7.9	4.1[a]
Sch.2	eV	4.5	5.7	5.7	4.9	4.2	7.0	5.1	6.0	3.0	6.0	5.6	4.2	0.7	5.0	3.9	2.5	3.3	3.5	8.2	4.23[a]
Sch.3	eV	5.0	6.5	5.5	4.6	4.8	7.2	4.7	5.6	3.0	6.5	6.3	4.3	0.8	4.3	4.2	2.5	3.6	3.7	9.2	6–7
Migration energies																					
O_I mig	eV	0.7	1.3	0.8	[c]	3.6	1.1	0.7	0.5	0.5	0.2	[c]	[c]	0.1	0.7	0.7	0.1	0.5	0.3	1.3	0.9 – 1.3
O_I mig2	eV	0.7	1.3	0.8	[d]	[c]	1.1	0.7	0.8	0.3	0.2	[d]	[d]	.4	0.7	0.7	0.1	0.5	0.4	1.3	
V_O mig	eV	0.3	0.3	0.3	0.5	0.3	0.7	0.6	0.6	0.1	0.5	0.5	0.5	0.2	0.5	0.3	0.1	0.2	0.2	0.4	0.5
U_I mig	eV	[c]	5.1	1.3	4.2	3.7	[d]	4.4	[d]	[c]	1.8	1.3	5.2	[d]	1.3	4.2	3.2	[c]	4.4	5.1	4.4–5.6
U_I mig2	eV	6.5	6.4	[d]	4.4	3.7	[d]	4.9	[d]	[d]	7.2	9.6	5.2	2.2	4.5	4.2	[d]	3.1	5.6	3.9	4.4–5.6
V_U mig	eV	5.6	5.7	8.2	3.7	3.1	6.8	5.2	0.6	3.9	6.2	4.4	2.8	3.7	4.5	3.9	0.9	5.7	5.2	6.4	
Binding energies																					
2 V_O	eV	−2.5	−2.6	−1.8	−1.4	−1.4	−2.2	−1.4	−1.3	−1.8	−2.5	−1.7	−1.9	−2.2	−1.2	−1.5	−1.7	−2.3	−2.2	−2.9	
$V_O + V_U$	eV	3.0	3.0	2.4	2.3	1.8	3.3	2.4	2.5	1.9	3.5	2.4	2.5	1.5	2.2	2.1	1.7	2.4	2.5	3.2	0.4[a]
2 O_I	eV	−0.8	−1.0	−0.1	[d]	0.6	−0.8	−0.2	−0.4	0.0	−1.3	−0.6	−0.6	0.4	−0.3	−0.9	0.3	−0.4	−0.4	−1.0	
2 O_I [b]	eV	−0.8	−1.0	0.0	[d]	0.7	−0.7	−0.1	−0.4	0.0	−1.3	−0.7	−0.6	−17.9	−0.2	−0.9	0.1	−0.2	−0.3	−0.9	
4-vac.	eV	7.6	7.5	6.9	6.6	5.0	9.2	6.7	7.2	5.0	9.0	6.5	6.5	3.7	6.4	5.6	4.6	6.2	6.1	8.0	

[a] Ab initio data.

[b] Spheres radii were 14 and 24 Å.

[c] Negative migration energy.

[d] Minimum of energy not found.

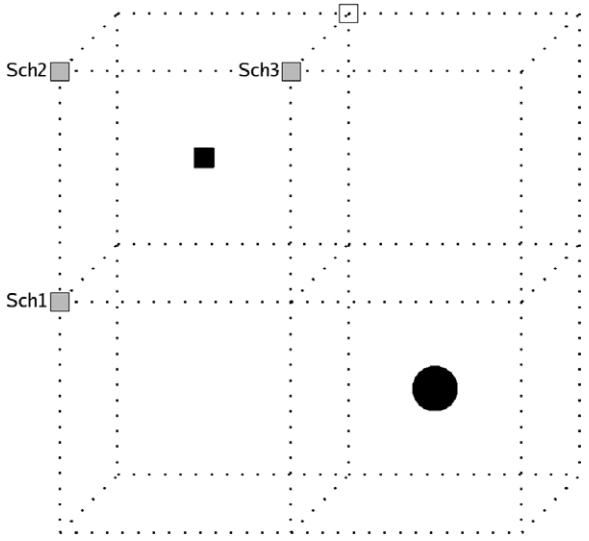

Fig. 2. Different Schottky configurations envisaged. Dark spheres are U atoms. O atoms are situated at each gray cube edge, but not depicted for clarity reasons. The dark square is the U vacancy, the white square is the first oxygen vacancy, and the gray square are the different configuration of the second oxygen vacancy.

2.3.4. Defect migration energies

Experimental values of oxygen, uranium vacancies and interstitials migration energies – V_O, V_U, O_I, U_I mig – can be found in [61,62,64,65,74–77]. The prediction of migration energies was done by searching an energy saddle point when an atom was removed (vacancy migration) or added (interstitial migration). This search can become difficult when many saddle points are very close to each other. In such cases a better solution is to impose the position of the migrating ion, or to sample the energy when an atom follows a specific migration path. The first approach has been used in this article because no migration pathway is imposed or guessed, even if for that reason there is no guarantee that the atomic configurations are the same for all potentials. The migration energy of interstitials was evaluated using two different initial conditions (small initial displacement in the $\langle 1\,0\,0\rangle$ and $\langle 1\,1\,0\rangle$ directions for respectively the first and second values reported in Table 4) using the RFO method in order to find a saddle point. If these values were not very close to each other, we deduced that the saddle point is difficult to search (e.g. many saddle points and local minima near the configuration) and no value is then provided in the table. In the case of vacancy migration this problem did not appear.

The radii of the two spheres in the Mott–Littleton approach were of 9 and 20 Å. A convergence test was done calculating the same energies with radii of 14 and 24 Å. A noticeable difference was only observed for close Frenkel defects. The distance between the interstitial and the vacancy is in this case of about 7 Å, which explains that a full relaxation in a sphere of 9 Å radius is not sufficient.

The calculation results for all potentials can be found in Table 4, all calculations were performed with radii of 9 and 20 Å. For close Frenkel pairs, 14 and 24 Å radii were used.

2.3.5. Relaxation volume around defects

We have selected some of these potentials, taken to be representative of their 'class', namely for rigid ion potentials with formal charges: Arima1 [43], Karakasidis [23], Lewis_a [12] and Walker [10]; for rigid ion potentials with non-formal charges: Basak [42] (charges -1.2 and $2.4e$ for O and U) and Morelon [24] (charges ≈ -1.6 and $\approx 3.2e$); for the shell–core potentials: Catlow1 [6], Grimes [28], Jackson1 [14], Jackson2 [14], Lewis_b [12] and Meis2 [45] potentials.

These potentials were used to determine the relaxation volume (difference of volume between the system containing no defect and the system containing one or more defects) around neutral trivacancies, oxygen interstitials, vacancies and Frenkel pairs. It was achieved using periodic boundary conditions and working at zero pressure. The system consisted into $4\times4\times4$ primitive unit cells (768 atoms) and defects were created removing and/or adding atoms manually. Other box sizes have been considered ($2\times2\times2$; $3\times3\times3$; $6\times6\times6$) with one of the potentials, in order to assess box size influence on the results. Relaxation volumes were almost identical.

The minimisation used a conjugate gradient algorithm. Electroneutrality in the box was maintained by adding a uniform background charge. This uniform charge only results in a modification of the energy of the box without changing the forces due to the defect and its images. These results can be found in Table 5. They are compared to volume changes calculated ab initio by Freyss and Petit [70] in the Generalized Gradient Approximation (GGA). As these calculations predicted a metallic behaviour for UO_2, no charged cells could be simulated, even when considering interstitials and vacancies. Ab initio calculations are very time-consuming and for this reason small unit cells were used

Table 5
Relaxation volume Å^3, predicted by different potentials using a box of $4\times4\times4$ unit cells (768 atoms)

Number of defects	Potentials												
	Arima1 [43]	Basak [42]	Catlow2 [6]	Grimes [28]	Jackson1 [13]	Jackson2 [13]	Karakasidis [23]	Lewis_a [12]	Lewis_b [12]	Meis2 [45]	Morelon [24]	Walker [10]	ab initio [70]
Oxygen interstitial													
1	9.0	16.2	9.8	6.5	5.5	3.3	5.7	5.4	4.8	–	2.4	7.4	
2	17.5	32.0	20.4	12.7	10.6	6.3	11.1	10.6	8.8	10.1	4.2	14.4	
4	35.2	73.0	40.3	25.2	21.3	12.3	22.4	20.8	–	18.6	8.2	–	
6	67.2	115.5	60.7	36.6	33.1	17.8	–	29.3	–	29.0	10.2	–	
8	96.2	164.1	81.0	48.2	41.9	24.9	–	37.1	–	39.1	12.9	–	
$\overline{\Delta V}/O_I$	12.0	20.5	10.1	6.0	5.3	3.0	5.6	4.7	4.4	4.9	1.6	7.2	5–1
Oxygen vacancy													
1	−1.3	−5.3	−1.6	−1.6	−2.2	−1.6	−0.0	0.0	−0.4	0.1	1.7	−0.3	
2	−3.0	−11.2	−3.6	−3.4	−1.8	−3.1	−0.4	−0.4	−1.2	0.0	3.1	−1.1	
4	−6.0	−22.5	−7.3	−7.0	−2.8	−4.4	−1.2	−0.9	−3.0	−0.2	6.0	−2.0	
6	−10.0	−34.8	−13.7	−12.3	−6.2	−8.3	−2.4	−2.5	−5.7	−2.1	7.8	−3.5	
8	−17.3	−49.9	–	−17.8	−11.5	−11.8	−7.5	−6.6	−10.1	−4.7	7.3	−8.6	
$\overline{\Delta V}/V_O$	−2.1	−6.2	−2.2	−2.2	−1.3	−1.4	−0.8	−0.8	−1.2	−0.6	1.0	−1.0	3–29
Trivacancy													
1	8.0	14.0	4.8	−4.4	1.4	−1.9	7.2	6.0	4.7	4.1	5.4	8.4	
2	17.5	19.2	10.8	32.2	10.1	4.5	13.4	14.3	10.6	9.4	17.9	19.4	
4	42.7	35.7	27.3	2.9	26.8	18.4	41.1	32.8	30.4	31.5	28.9	47.3	
$\overline{\Delta V}$/Triv.	10.8	8.5	6.9	–	7.1	5.0	10.3	8.3	7.7	8.0	7.5	12.0	
Oxygen Frenkel pair													
1	8.5	11.3	6.8	5.1	5.3	2.4	6.2	6.2	4.8	5.3	4.8	9.4	
2	17.9	23.7	19.3	11.0	10.9	5.5	13.2	12.4	–	11.7	10.0	30.0	
$\overline{\Delta V}$/OFP	8.9	11.9	9.6	5.5	5.4	2.8	6.6	6.2	4.8	5.9	5.0	15.0	

Note: (–) means that this value could not be calculated.

($1\times1\times1$ and $1\times1\times2$ boxes), and only volume changes associated with vacancies and interstitials were calculated.

3. Discussion

In this section, we compare the results in Table 4 obtained with the different potentials and we discuss discrepancies pertaining their range of applicability in static calculations.

3.1. Cohesive energy

As for the determination of vacancies or interstitials formation energies, the determination of the cohesive energy of an ionic crystal depends on the reference energy used (see Section 2.3.3). When using interatomic potentials with fixed ion charges, the zero level is obtained when all charged ions are at infinite distance from each other. Potentials with non-formal charges will thus not have the same reference state (e.g. $O^{-1.2}$ and $U^{2.4}$ atoms at ∞) as potentials with formal charges (O^{-2} and U^{4} at ∞). The electrostatic potential providing about 90% of the cohesive energy, a large difference is expected between potentials with non-formal charges and those with formal charges.

3.2. Elastic properties

It appears that elastic constants (C_{11}, C_{12}, C_{44}, B, E) at 0 K are generally well reproduced by all potentials. This is not surprising since they are generally developed by fitting to these values. Even if it was expected, it confirms that no error was made in the interpretation of the parameters and their units reported by the different authors. Indeed in some articles units were not given [35,43] or were inconsistent [42]. Two potentials (Grimes [28], Morelon [24]) were not based on elastic properties fitting and, in these cases, the calculation of elastic constants can be considered as independent estimations. The basis for development of the Grimes [28] potential were electron-gas calculations. The Morelon [24] potential was fitted on the lattice parameter, its evolution with temperature and in order to reproduce defect

energies, as mentioned. The results obtained by the Grimes potential [28] slightly overestimate elastic properties and by Morelon [24] underestimate them.

Since polarisability is not incorporated in rigid ion potentials, they will always predict a high-frequency dielectric constant of 1, which is quite far from the experimental value of 5.3. The main consequence of it appears in the optical phonon modes, which are thus only accurately described by the shell–core potentials.

3.3. Defect energies

3.3.1. Formation energies

Globally all potentials give the same trend for all defect energies. The comparison to experimental data or to ab initio results is not directly possible in case of charged defects, as it was argued in Section 2.3.3. Therefore, only neutral defects, binding energies and migration energies have been computed.

Frenkel pair formation energies calculated by interatomic potentials or ab initio techniques are generally expressed as the sum of interstitial and vacancy formation energies and compared to experimental values. From Table 4 it appears that the oxygen Frenkel pair (OFP) formation energies calculated using potentials developed only on lattice properties are slightly higher than the experimental values. When OFP are calculated as an interstitial close to a vacancy (close Frenkel pairs), almost all potential predict an OFP value in the experimental range, with the exception of Grimes potential which still slightly overestimates it. This situation should correspond to what is measured experimentally, because an atom leaving its regular place will initially be in its neighborhood. Recent ab initio calculations by Gupta et al. [72] also provide Frenkel pair energies at large, medium and small distance.

The same tendency occurs for uranium Frenkel pairs (UFP) and for Schottky defects. Conclusions for UFP are more difficult to make because experimental values are thought to underestimate the real value [24,68]. More confidence can be found in ab initio results for this type of value.

3.3.2. Migration energies

Two calculations with different initial displacement of the migrating atom were performed in the case of interstitials. A concordance of the results indicates that the saddle point is well determined, while different values indicated a problem in finding the saddle point: in some cases a negative activation energy was predicted for a particular initial condition, which, is due to the attractive form of Buckingham potential at small distances. A visualisation of the results obtained with the Lewis_b potential showed that two oxygen atoms have their shell situated at less than 1 Å form the other's core and from each other.

Note that the migration energy calculated with the second initial condition was nevertheless positive or could not be found, denoting a problem for these specific calculations.

An analysis of the saddle point configurations showed that the predicted mechanism for oxygen interstitial migration is an interstitialcy mechanism, as illustrated in Fig. 3. This was observed for most potentials, with the exception of the problematic ones above mentioned. The migration of oxygen vacancies is predicted to consist of oxygen motion along the $\langle 100 \rangle$ direction.

For uranium defects, the situation was more complicated. A number of potentials (Arima1, Basak, Busker, Jackson1, Lewis_b, Meis2, Morelon, Yamada) tend to predict a $\langle 100 \rangle$ motion of the interstitial (see Fig. 4), the Walker potential indicates a $\langle 110 \rangle$ motion, while for the other potentials, the mechanism is not clear. The uranium vacancy

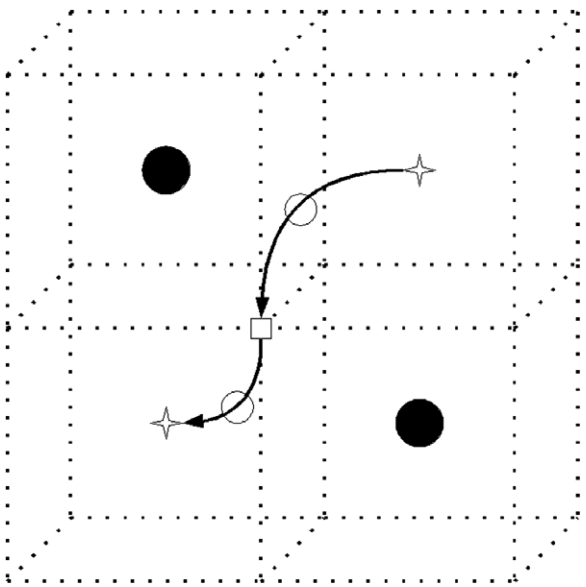

Fig. 3. Interstitialcy mechanism for oxygen atoms. Dark spheres are U atoms. Regular O atoms are situated at each gray cube edge, but are not depicted for clarity reasons. The stars indicate interstitial sites, the white square is an oxygen vacancy, white spheres are migrating oxygen atoms.

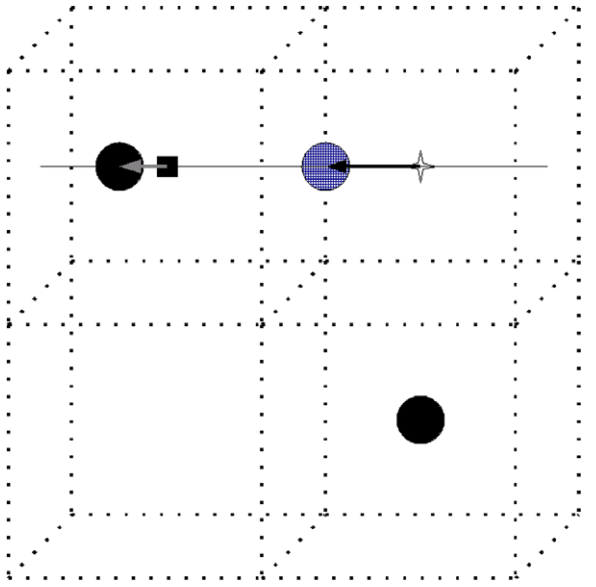

Fig. 4. Uranium interstitial migration mechanism. Dark spheres are U atoms. Regular O atoms are situated at each gray cube edge, but are not depicted for clarity reasons. The stars indicate interstitial sites, the dark square is an uranium vacancy, and the crossed sphere the uranium interstitial.

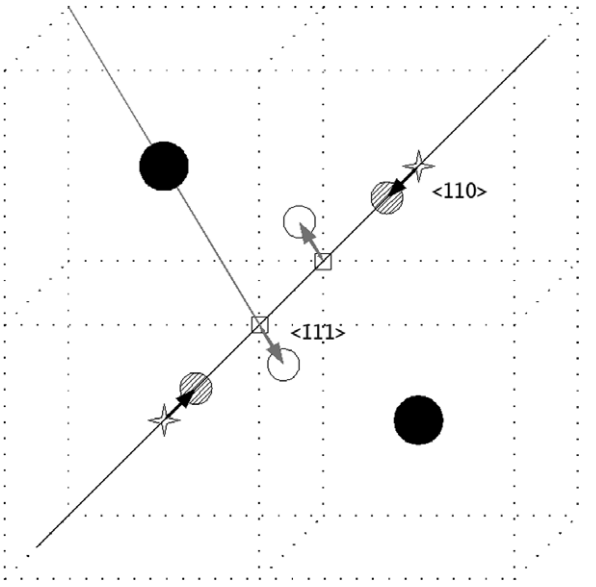

Fig. 5. Willis clusters. Dark spheres are U atoms. Regular O atoms are situated at each gray cube edge, but are not depicted for clarity reasons. The stars indicate interstitial sites, white squares are oxygen vacancies, white spheres are regular oxygen atoms displaced from their original site, and hashed spheres are the two oxygen interstitials.

migration is generally predicted to occur in the $\langle 1\,1\,0\rangle$ direction.

3.3.3. Binding energies

Binding energy calculations allow comparing clustering predictions with different potentials. It appears that two oxygen vacancies repel each other, while the different combinations of oxygen and uranium vacancies ($V_O + V_U$; $2V_O + V_U$; $2V_O + 2V_U$) are bound.

Clusters of two oxygen interstitials experimentally appear under the form of Willis clusters [78]. They consist of two oxygen interstitials displaced in the $\langle 1\,1\,0\rangle$ direction from the oxygen cube center and the displacement of two regular oxygen atoms in the $\langle 1\,1\,1\rangle$ direction. This situation is depicted in Fig. 5.

Willis clusters were only predicted using energy minimisation by three potentials: Catlow2, Karakasidis and Sindzingre. However, it appeared from MD simulations of these clusters that the state found with all potentials was not the most stable one (this configuration can be seen in Fig. 6). After reaching the structure predicted with energy minimisation, the thermal motion allowed to go to a deeper minimum. Its structure for most potentials consisted of three oxygen interstitials and one oxygen vacancy

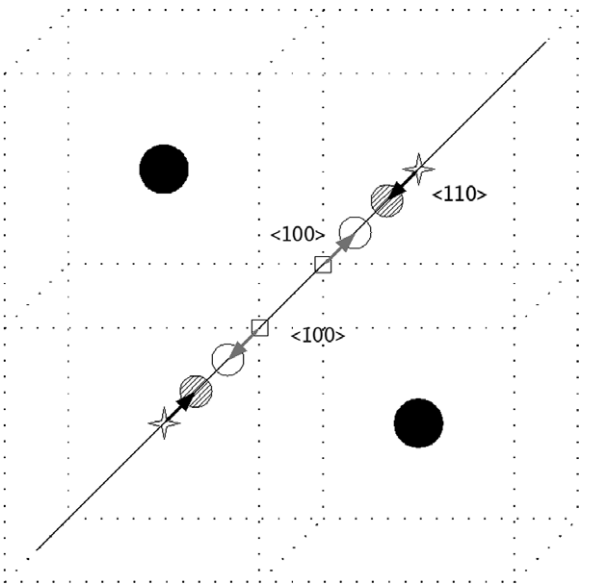

Fig. 6. Di-interstitial cluster predicted by static calculations. Dark spheres are U atoms. Regular O atoms are situated at each gray cube edge, but are not depicted for clarity reasons. The stars indicate interstitial sites, white squares are oxygen vacancies, white spheres are regular oxygen atoms displaced from their original site, and hashed spheres are the two oxygen interstitials.

(see Fig. 7). This structure has a positive binding energy. One important point to note is that in these simulations oxygen and uranium valences are not allowed to vary with the environment, which means that local electroneutrality is not maintained. Catlow [6] modelled Willis clusters with modified uranium charges in order to compensate, at least partially, the charge of the oxygen interstitials. These charge modifications with the local environment can be considered in static calculations but are actually inapplicable in the course of MD simulations.

Another problem may occur for the simulation of oxygen interstitials, as observed by Crocombette in zirconium orthosilicate [79]. The study of oxygen interstitials by interatomic potentials and by ab initio calculations predicted very different behaviours: the ab initio calculations predicted that an O_2 molecule is formed at a regular oxygen site in the lattice. This is impossible to simulate with interatomic potentials as two oxygen will repulse each other because of their identical charges. This effect has not been reported for oxygen interstitials in UO_2, but it cannot actually be excluded for clusters of oxygen interstitials.

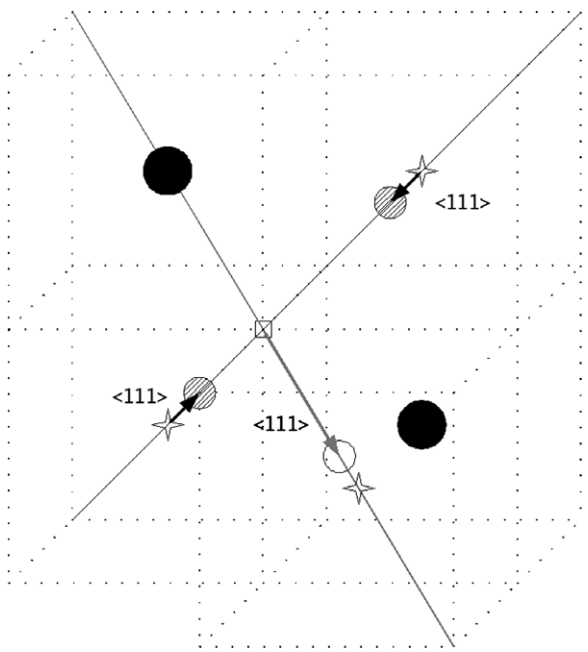

Fig. 7. Di-interstitial cluster predicted by MD simulations. Dark spheres are U atoms. Regular O atoms are situated at each gray cube edge, but are not depicted for clarity reasons. The stars indicate interstitial sites, the white square is an oxygen vacancy, the white spheres is a regular oxygen atom displaced from its original site, and hashed spheres are the two oxygen interstitials.

3.4. Relaxation volume

Volume changes are reported in Table 5 and compared to ab initio results obtained with much smaller boxes. We have to keep in mind that in ab initio calculations, the sum of all atoms charges was zero for O_I and V_O, while in our simulations the uniform background charge added only modifies the energy reference, not the electrostatic forces between atoms. The defect interacts with its images produced by the periodic boundary conditions, which can affect the results for too small boxes (such as if the same size as ab initio calculations was used) or if too many charged defects are present.

The different potentials predict a relaxation volume associated with oxygen interstitials of 3–10 $Å^3$, in good agreement with ab initio results, with the exception of Morelon potential (1.6 $Å^3$), Arima1 (12 $Å^3$) and Basak (20.5 $Å^3$). It is well-known and long established experimentally [80] that hyperstoichiometric fuel shows a decrease of lattice parameter with departure from stoichiometry. This is in contradiction with all calculated results that predict swelling with increased concentration of oxygen interstitials.

The prediction of swelling due to isolated oxygen interstitials can be questioned as Willis clusters are observed experimentally. For this reason we have computed volume change associated to Willis clusters with one of the potentials that predicted their formation: the Catlow2 potential. It is reported in Table 6. Relaxation volumes are again positive.

A possible explanation for these unphysical results may be found in the way electroneutrality is achieved in MD calculations, adding an uniform background charge. Another way of maintaining electroneutrality, but in this case more locally, is to modify the uranium atoms charge around an oxygen vacancy, an oxygen interstitial or in the

Table 6
Comparison of the relaxation volume associated with oxygen interstitials and Willis clusters. Calculations done with Catlow2 potential

Number of O_I	Uniformly distributed	Willis clusters
1	9.8	
2	20.4	25.5
4	40.3	49.0
6	60.7	74.7
8	81.0	98.2
$\overline{\Delta V}/O_I$	10.1	12.3

Willis cluster structure. An estimation of the relaxation volume of isolated U^{3+} (compensating positively charged defects) and U^{5+} (compensating negatively charged defects) has been calculated with three potentials (Catlow2, Karakasidis and Lewis_a). The parameters of the O–U interatomic potential were not modified for these two ions, only their charge; this approximation is not expected to have an important influence on the results. The volume change calculated were ≈ 10 Å^3 for U^{3+} and ≈ -10 Å^3 for U^{5+}. These results suggest that the major contribution to the swelling dependence on stoichiometry may be due to electrons and holes compensating the charge of a defect, located on uranium atom sites.

This result questions the validity of estimating the relaxation volume of charged defects if the local electroneutrality is not maintained.

Oxygen vacancies are predicted to result in a contraction of the lattice except for Morelon potential and for 1 or 2 defects by the Meis2 potential, that agree with ab initio data. Basak potential, which gave in the previous calculations good predictions on elastic and defect data predicts here results about twice higher than all other potentials. Oxygen Frenkel pairs are predicted to have a relaxation volume of 5–10 Å^3 for all potentials.

An interesting prediction of all potentials is that trivacancies also induce a swelling of the matrix. The relaxation volume associated to it lies between 5 and 12 Å^3.

4. Synthesis

The aim of this study was to assess the range of applicability of the existing interatomic potentials developed for the UO_2 system. The main concretisation of this work can be found in Table 4 (comparison of elastic properties and various energies associated with defects) and in Table 5 (comparison of volume change associated with trivacancies, oxygen vacancies, oxygen interstitials and oxygen Frenkel pairs).

The elastic properties are generally accurately reproduced, mainly because these values were part of the fitting parameters used by most of the developers of pair potentials. Only one potential [24] was, intentionally, not fitted to elastic data and slightly underestimate them. Another potential [28] was developed on the theoretical basis of electron-gas calculations. This potential slightly overestimated elastic properties.

With regard to defect formation energies (oxygen, uranium Frenkel pairs; Schottky defects) an appreciable variation of the energy according to the envisaged configuration was observed. 'Close' configurations of defects were predicted to be more stable than defects at infinite distance from each other by 1–2 eV for the oxygen Frenkel pair, 3–5 eV for the uranium Frenkel pair and 3–6 eV for the Schottky defect. Depending on the configuration chosen to be compared to experimental data, most potentials will be considered as 'applicable' (close configuration) or 'rejected' (large separation of defects) for the modelling of defects.

The binding energies of clusters were calculated. Difficulties were encountered for oxygen di-interstitials. Energy minimisation calculations predicted the (2:2:2) structure of Willis clusters for three potentials. MD simulations, even at low temperature, allowed to find a deeper minimum thanks to thermal motion, whose structure consisted of three oxygen interstitials and one oxygen vacancy for most of the potentials. The Yamada potential predicted a different structure with a small displacement of six regular oxygen atoms around the two interstitials. These results have to be taken carefully as no charge compensation by uranium atoms was used in the Willis cluster structure in order to compensate, even partially, the additional charges of oxygen interstitials.

The migration energies will play an important role e.g. for the consideration of defects recombination. The calculations of these quantities predicted a different behaviour from one potential to the other one. The migration of interstitials were in some cases difficult to search, which is evidenced by different migration energies obtained with small perturbations in the initial condition of the saddle-point search.

Finally, the relaxation volume around the dominant defects of UO_2 has been envisaged in this study, in a first time maintaining electroneutrality with a uniform background charge, which physically only results in a modification of the system energy. Since each type of defect was studied separately, these calculations do not really permit to compare the predictions of the potentials with experimental values, but they indicate the relative contribution of each type of defect to the lattice parameter change. A swelling induced by oxygen interstitials is predicted by all potentials, while it is experimentally known that hyperstoichiometry results in a contraction of the lattice. Therefore we

also considered Willis clusters in our calculations. Their positive relaxation volume is also incompatible with a lattice contraction for hyperstoichiometric fuels.

Electroneutrality was maintained adding an uniform background charge; but it can also be maintained more locally by modification of the uranium valence. It seems from our estimations of relaxation volume around localized electron or holes (U^{3+} and U^{5+}) that this type of charge compensation would provide the major contribution to lattice parameter change, and would explain the evolution of the lattice parameter with the deviation from stoichiometry. A second interesting result of this work is the positive relaxation volume induced by trivacancies.

Determining from these results a single best, or most accurate, potential is impossible. Our study shows that differences appeared when considering complex situations (migration of defects, clusters). Moreover, the results indicate that the classes of potential (shell–core, rigid ion), the type of potential (Buckingham, Buckingham-4-ranges, Morse), neither the percentage of ionicity attributed to ions, but the fitted parameters themselves (and the observables on which they are fitted) have an important influence on the accuracy of the potential.

We might be in a better position to make a selection of the most accurate potential after full MD calculations at non-zero temperatures. Hence, the next steps of this study will concern the evolution of different quantities (lattice parameter, specific heat, bulk modulus, etc.) with temperature, predicted by all these potentials. This will provide useful information to assess the applicability of these potentials for dynamic events.

References

[1] B.G. Dick, A.W. Overhauser, Phys. Rev. 112 (1958) 90.
[2] G.C. Benson, P.I. Freeman, E. Dempsey, J. Am. Ceram. Soc. 46 (1962) 43.
[3] G. Dolling, R.A. Cowley, A.D. Woods, Can. J. Phys. 43 (1965) 1397.
[4] K. Tharmalingam, Philos. Mag. 23 (1971) 199.
[5] C.R.A. Catlow, M.J. Norgett, J. de Phys. Coll. C9 34 (1973) 45.
[6] C.R.A. Catlow, Proc. R. Soc. Lond. A. 353 (1977) 533.
[7] C.R.A. Catlow, Proc. R. Soc. Lond. A. 364 (1978) 473.
[8] M. Sugisaki, J. Nucl. Mater. 79 (1979) 338.
[9] M. Abramowski, R.W. Grimes, S. Owens, J. Nucl. Mater. 275 (1999) 12.
[10] J.R. Walker, C.R.A. Catlow, J. Phys. C: Solid State Phys. 14 (1981) L979.
[11] S. Motoyama, Y. Ichikawa, Y. Hiwatari, A. Oe, Phys. Rev. B 60 (1999) 292.
[12] G.V. Lewis, C.R.A. Catlow, J. Phys. C: Solid State Phys. 18 (1985) 1149.
[13] R.A. Jackson, A.D. Murray, C.R.A. Catlow, Physica B 131 (1985) 136.
[14] R.A. Jackson, A.D. Murray, J.H. Harding, C.R.A. Catlow, Philos. Mag. A 53 (1986) 27.
[15] R.A. Jackson, C.R.A. Catlow, J. Nucl. Mater. 127 (1985) 161.
[16] R.A. Jackson, C.R.A. Catlow, J. Nucl. Mater. 127 (1985) 167.
[17] P.J.D. Lindan, M.J. Gillan, Philos. Mag. B 69 (1994) 535.
[18] S. Nicoll, H. Matzke, C.R.A. Catlow, J. Nucl. Mater. 226 (1995) 51.
[19] S. Nicoll, H. Matzke, R.W. Grimes, C.R.A. Catlow, J. Nucl. Mater. 240 (1997) 185.
[20] P. Sindzingre, M.J. Gillan, J. Phys. C: Solid State Phys. 21 (1988) 4017.
[21] M.J. Gillan, Mol. Simul. 3 (1989) 15.
[22] P.J.D. Lindan, M.J. Gillan, J. Phys.: Condens. Matter 3 (1991) 3929.
[23] T. Karakasidis, P.J.D. Lindan, J. Phys.: Condens. Matter 6 (1994) 2965.
[24] N.-D. Morelon, D. Ghaleb, J.-M. Delhaye, L. Van Brutzel, Philos. Mag. 83 (2003) 1533.
[25] L. Van Brutzel, J.-M. Delhaye, D. Ghaleb, M. Rarivomanantsoa, Philos. Mag. 83 (2003) 4083.
[26] R.W. Grimes, C.R.A. Catlow, J. Am. Ceram. Soc. 72 (1989) 1856.
[27] C.R.A. Catlow, R.W. Grimes, J. Nucl. Mater. 165 (1989) 313.
[28] R.W. Grimes, C.R.A. Catlow, Philos. Trans. R. Soc. Lond. A 335 (1991) 609.
[29] R.W. Grimes, R.H. Miller, C.R.A. Catlow, J. Nucl. Mater. 172 (1990) 123.
[30] R.G.J. Ball, R.W. Grimes, J. Chem. Soc. Faraday Trans. 86 (1990) 1257.
[31] R.W. Grimes, R.G.J. Ball, C.R.A. Catlow, J. Phys. Chem. Solids 53 (1992) 475.
[32] R.W. Grimes, Mat. Res. Soc. Symp. Proc. 257 (1992) 361.
[33] G. Busker, R.W. Grimes, M.R. Bradford, J. Nucl. Mater. 279 (2000) 46.
[34] G. Busker, R.W. Grimes, M.R. Bradford, J. Nucl. Mater. 312 (2003) 156.
[35] K. Yamada, K. Kurosaki, M. Uno, S. Yamanaka, J. Alloys Compd. 307 (2000) 10.
[36] K. Kurosaki, K. Yamada, M. Uno, S. Yamanaka, K. Yamamoto, T. Namekawa, J. Nucl. Mater. 294 (2001) 160.
[37] K. Kurosaki, M. Imamura, I. Sato, T. Namekawa, M. Uno, S. Yamanaka, J. Nucl. Sci. Tech. 41 (2004) 827.
[38] K. Kurosaki, M. Imamura, I. Sato, T. Namekawa, M. Uno, S. Yamanaka, J. Alloys. Compd. 387 (2005) 9.
[39] K. Kurosaki, K. Yano, K. Yamada, M. Uno, S. Yamanaka, J. Alloys. Compd. 311 (2000) 305.
[40] K. Kurosaki, K. Yano, K. Yamada, M. Uno, S. Yamanaka, J. Alloys. Compd. 313 (2000) 242.
[41] K. Kurosaki, J. Adachi, M. Uno, S. Yamanaka, J. Nucl. Mater. 344 (2005) 45.
[42] C.B. Basak, A.K. Sengupta, H.S. Kamath, J. Alloys. Compd. 360 (2003) 210.

[43] T. Arima, S. Yamasaki, Y. Inagaki, K. Idemitsu, J. Alloys. Compd. 400 (2005) 43.
[44] C. Meis, J.D. Gale, Mater. Sci. Eng. B 57 (1998) 52.
[45] C. Meis, A. Chartier, J. Nucl. Mater. 341 (2005) 25.
[46] N.F. Mott, M.J. Littleton, Trans. Faraday Soc. 34 (1938) 485.
[47] J.D. Gale, A.L. Rohl, Mol. Simul. 29 (2003) 291.
[48] A. Banerjee, N. Adams, J. Simons, R. Shepard, J. Phys. Chem. 89 (1985) 52.
[49] J.K. Fink, J. Nucl. Mater. 279 (2000) 1.
[50] M.T. Hutchings, J. Chem. Soc. Faraday Trans. 2 (83) (1987) 1083.
[51] A. Padel, C. de Novion, J. Nucl. Mater. 33 (1969) 40.
[52] K. Clausen, W. Hayes, M.T. Hutchings, J.E. Macdonald, R. Osborn, P. Schnabel, Rev. Phys. Appl. 19 (1984) 719.
[53] K. Clausen, W. Hayes, J.E. Macdonald, R. Osborn, Phys. Rev. Lett. 52 (1984) 1238.
[54] D.G. Martin, High Temp. High Press. 21 (1989) 13.
[55] K. Clausen, W. Hayes, M.T. Hutchings, J.K. Kjems, J.E. Macdonald, R. Osborn, High Temp. Sci. 19 (1985) 189.
[56] I.J. Fritz, J. Appl. Phys. 47 (1976) 4353.
[57] M.O. Marlowe, J. Nucl. Mater. 33 (1969) 242.
[58] J.B. Wachtman, M.L. Wheat, H.J. Anderson, J.L. Bates, J. Nucl. Mater. 16 (1964) 39.
[59] R.J. Ackermann, R.J. Thorn, G.M. Winslow, J. Opt. Soc. Am. 49 (1959) 1107.
[60] K.N. Clausen, M.A. Hackett, W. Hayes, S. Hull, M.T. Hutchings, J.E. MacDonald, K.A. McEwen, Physica B 156 (1989) 103.
[61] H. Matzke, J. Chem. Soc. Faraday Trans. 2 (83) (1987) 1121.
[62] K.C. Kim, D.R. Olander, J. Nucl. Mater. 102 (1981) 192.
[63] R. Swarc, J. Phys. Chem. Solids 30 (1969) 705.
[64] J. Belle, A.B. Auskern, W.A. Bostrom, F.S. Susko, in: Proc. 4th. Int. Symp. of React. of Solids, 1961, p. 452.
[65] H. Matzke, J. Phys. C9 34 (1973) 317.
[66] D. Vollath, in: Proc Reaktoragung, 1971, p. 558.
[67] T. Petit, C. Lemaignan, F. Jollet, B. Bigot, A. Pasturel, Philos. Mag. B 77 (1998) 779.
[68] J.P. Crocombette, F. Jollet, L. Thien Nga, T. Petit, Phys. Rev. B 64 (2001) 104107.
[69] T. Petit, M. Freyss, P. Garcia, P. Martin, M. Ripert, J.P. Crocombette, F. Jollet, J. Nucl. Mater. 320 (2003) 133.
[70] M. Freyss, T. Petit, J.P. Crocombette, J. Nucl. Mater. 347 (2005) 44.
[71] M. Freyss, N. Vergnet, T. Petit, J. Nucl. Mater. 352 (2006) 144.
[72] F. Gupta, A. Pasturel, G. Brillant, in: 5th Workshop, Nice, France, 2006.
[73] J. Mayer, M. Fähnle, Acta Mater. 45 (1997) 2207.
[74] P. Contamin, J.J. Bacmann, J.F. Marin, J. Nucl. Mater. 42 (1972) 54.
[75] J. Belle, J. Nucl. Mater. 30 (1969) 3.
[76] J.F. Marin, P. Contamin, J. Nucl. Mater. 30 (1969) 16.
[77] H. Matzke, J. Nucl. Mater. 30 (1969) 26.
[78] B.T.M. Willis, Proc. Br. Ceram. Soc. 1 (1964) 9.
[79] J.P. Crocombette, Phys. Chem. Miner. 27 (1999) 138.
[80] L. Lynds, W.A. Young, J.S. Mohl, G.G. Libowitz, Adv. Chem. 39 (1962) 58.